J Solid State Electrochem (2012) 16:2555–2561
DOI 10.1007/s10008-012-1659-x

ORIGINAL PAPER

Synthesis of γ-LiV_2O_5 nanorods as a high-performance cathode for Li ion battery

Wenjie Wang · Haiyan Wang · Suqin Liu · Jianhan Huang

Received: 18 November 2011 / Revised: 11 January 2012 / Accepted: 14 January 2012 / Published online: 17 February 2012

Abstract One-dimension γ-LiV_2O_5 nanorods were synthesized using VO_2(B) nanorods as precursor in this study. The as-prepared material is characterized by X-ray diffraction, X-ray photoelectron spectrometry, Fourier-transform infrared, transmission electron microscopy (TEM), cyclic voltammetry, and charge–discharge cycling test. TEM results show that LiV_2O_5 nanorods are 90–250 nm in diameter. The nanorods deliver a maximum discharge capacity of 284.3 mAh g^{-1} at 15 mA g^{-1} and 270.2 mAh g^{-1} is maintained at the 15th cycle. Good rate performance is also observed with the discharge capacity of 250.1 and 202.6 mAh g^{-1} at 50 and 300 mA g^{-1}, respectively. The capacity retention at 300 mA g^{-1} is 84.2% over 50 cycles. The Li^+ diffusion coefficient of LiV_2O_5 is calculated to be 10^{-10}–10^{-9} cm^2 s^{-1}. It is demonstrated that the nanorod morphology could greatly facilitate to shorten lithium ion diffusion pathways and increase the contact area between active material and electrolyte, resulting in high capacity and rate performance for LiV_2O_5.

Keywords Li ion battery · LiV_2O_5 nanorod · VO_2 (B) nanorod · Hydrothermal method

Introduction

Vanadium oxides and their derivatives have attracted much more attention as insertion electrode materials for rechargeable lithium batteries due to their high capacity, low cost, and easy synthesis characteristics [1–6]. Among these materials, vanadium pentoxide (V_2O_5) has been extensively studied [7–14]. Up to now, with the aim of improving its electrochemical performance, a number of methodologies have been employed to synthesize various nanostructured V_2O_5 (nanorod, nanobelt, nanotube, nanowire, etc.). V_2O_5 exhibits a high initial specific discharge capacity of 400 mAh g^{-1} [15]. However, limited cycling stability has become a big obstacle for its further research and probable application for Li ion battery [6].

It is well known that more than three Li ions could be inserted into the V_2O_5 host to form $Li_xV_2O_5$ and it undergoes several phase transformations depending on the amount of Li ion intercalation [16, 17]. When $x<0.1$, the α-phase appears. The ε-phase exists for $0.35<x<0.7$, δ-phase for $0.7<x<1$, γ-phase for $1<x<2$, and ω-phase for $2<x<3$. It should be noted that the ω-phase will turn to irreversible rock salt-type structure when $x>3$. γ-LiV_2O_5 consists of a puckered layered framework in which Li ions are located between the $(VO_5)_n$ layers. As one of the promising cathode materials for Li ion battery, it has attracted lots of attention in recent years [18–23]. However, there are not too many reports for synthesis of this material because it is very difficult to prepare γ-LiV_2O_5, in which there are two valence states (V^{5+} and V^{4+}) of vanadium co-existing [20–23]. Murphy et al. [20] introduced a solution approach by the reaction of V_2O_5 with LiI in acetonitrile. However, its high cost made it not viable. Dai et al. [21] prepared γ-LiV_2O_5 after calcining the mixture of NH_4VO_3, LiOH, and CH_3-COOH at 350 °C. A solvothermal synthesis was developed to obtain γ-LiV_2O_5 nanorods by Wang et al., which showed poor cycling stability [22]. Barker et al. [23] fabricated γ-LiV_2O_5 by carbon reduction method, showing a stable reversible discharge capacity of 130 mAh g^{-1}

W. Wang · H. Wang · S. Liu (✉) · J. Huang
Key Laboratory of Resources Chemistry of Nonferrous Metals, Ministry of Education, College of Chemistry and Chemical Engineering, Central South University, Changsha 410083, People's Republic of China
e-mail: sqliu2003@126.com

between 2.8 and 3.8 V. Nevertheless, the available capacity in such voltage range is not enough for application in Li ion batteries.

Note that most of studies focused on the structure change to elucidate the lithium ion insertion/extraction mechanism. Only several papers involved the electrochemical performance of this kind of material [20–23]. Therefore, much work concerning preparation methods should be done to improve its electrochemical performance in terms of cycling stability and capacity. Herein, γ-LiV_2O_5 nanorods are synthesized by a facile hydrothermal method followed by a solid state process. In this paper, VO_2(B) nanorods are used as vanadium source. LiV_2O_5 nanorods exhibit a maximum discharge capacity of 284.3 mAh g^{-1} at 15 mA g^{-1} as well as good rate capability and cycling stability.

Experimental

Synthesis and characterization

All of the starting materials were of pure analytical grade and used directly without further purification. A typical hydrothermal method was employed to obtain the precursor of VO_2(B) nanorods [24]. A total of 0.73 g V_2O_5 and 20 ml *n*-butanol were added into distilled water and the mixture was stirred violently at about 50 °C. Then, the mixed solution with some insoluble intermediate was transferred into a 100-ml Teflon-lined stainless steel autoclave. The total volume of the solution was about 85 ml. The autoclave was sealed and heated at 180 °C for 48 h and then cooled to room temperature naturally. The obtained precipitate was collected by centrifugation and washed with distilled water and ethanol several times. The blue-black products were obtained after drying overnight at 110 °C in vacuum. Following that, 0.2 g as-prepared VO_2(B) and 0.0358 g $LiOH{\cdot}H_2O$ were added into a certain amount of methanol. After gentle stirring at room temperature for 2 h, the mixture solution was heated at 50 °C for 10 h to evaporate the methanol. The collected powder was then calcined at 300 °C for 10 h under Ar atmosphere.

The crystalline phases were identified by X-ray diffraction (XRD), which was carried out on a Rigaku D/Max 2500 VB + diffractometer utilizing a Cu-Kα source with a step of 0.02°. Fourier transform infrared (FT-IR) spectra were recorded using an Avatar 380 FT-IR spectrometer. X-ray photoelectron spectrometry (XPS) measurements were performed on a K-Alpha 1063 system with Al Kα radiation as the exciting source. Morphological studies were conducted using a JEOL-1230 transmission electron microscope (TEM) employing a LaB6 filament as the electron source.

Electrochemical measurements

The electrochemical cells were constructed by mixing the active material, polytetyafluoroethylene, and acetylene black in the weight ratio of 80:10:10. The above mixture was spread and pressed onto a steel stainless mesh (100 mesh) which served as a current collector. After solvent evaporation at room temperature and heating at 110 °C under vacuum for 12 h, the electrodes were assembled into CR2016 coin-type cells with commercial electrolyte (Guangzhou Tianci; 1 M $LiPF_6$ in 1:1, *v*/*v*, ethylene carbonate/dimethyl carbonate) and a Li metal as counter electrode. The cells were constructed in an Ar-filled MBraun glovebox and then cycled galvanostatically between 2.0 and 4.0 V (the voltage unit in this paper is versus Li/Li^+) at a desired current density with a Land CT2001A tester system at room temperature. Cyclic voltammetry (CV) was operated between 2.0 and 4.0 V using electrochemical station CHI600B with various scan rates (0.1, 0.2, 0.5, and 0.8 mV s^{-1}).

Results and discussion

Figure 1a shows the XRD pattern of as-prepared VO_2(B) precursor. As can be seen, the main diffraction peaks are in good agreement with those of the standard VO_2(B) PDF card (No. 81-2392). Besides, several impurity peaks due to V_3O_7 are observed. A slight amount of impurity could be accepted, which could finally turn to LiV_2O_5 after calcination with lithium source. The nanorod morphology of VO_2(B) is shown in Fig. 1b, c. The nanorods have an average diameter of 70–150 nm and length of several micrometers. Note that some of the nanorods attach together to form larger diameter and shorter length, revealing that the VO_2(B) nanorods are not well grown.

Figure 2 presents the XRD pattern of as-prepared LiV_2O_5. For comparison, the standard PDF card (No.18-0756) is also attached. All of the diffraction peaks can be easily indexed to orthorhombic LiV_2O_5 phase (space group P21/m). Meantime, it suggests high purity of the as-prepared material. The lattice parameters are calculated to be a=0.9039(1) nm, b=0.3655(2) nm, and c=1.0736(1) nm, which are a little different from those in literature [23]. It should be pointed out that the crystal volume of LiV_2O_5 is 0.3547 nm^3, which is much smaller than those values in the literature (0.3732 nm^3 for the standard PDF card and 0.3727 nm^3 for that by Barker et al. [23]). Crystal volume change is considered as an important reason for capacity fading with regard to electrode materials, especially at high current densities. Therefore, the structure of an electrode material with a less smaller crystal volume could be kept better during rapid Li ion insertion/extraction processes, which probably provides better cycling stability. As a matter

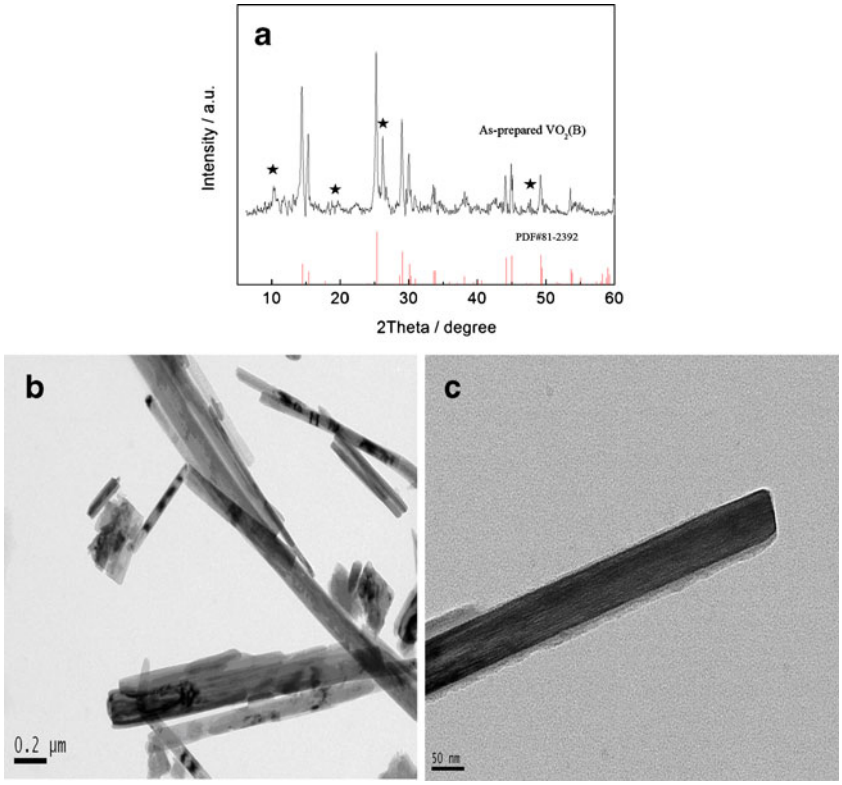

Fig. 1 XRD pattern (**a**) and TEM images (**b**, **c**) of as-prepared VO_2(B) precursor. The *asterisk* corresponds to the impurity of V_3O_7

of fact, the results agree well with the following electrochemical properties.

The chemical composition and valence state of V element in the products were further investigated by XPS. As presented in Fig. 3a, this sample only consists of vanadium, lithium, and oxygen elements. Note that carbon element in spectrum should be assigned to a small amount of carbon dioxide from the atmosphere absorbed on the surface of the products. There are two peaks at 517.5 and 524.8 eV in the V 2p core level spectrum (Fig. 3b), which are ascribed to the spin–orbit splitting of the components V 2p3/2 and V 2p1/2. The XPS region spectrum of V 2p3/2 in Fig. 3b consists of two overlapping peaks, 517.5 and 516.3 eV, which are in agreement with the results of V_2O_5 and VO_2, respectively [25]. Therefore, vanadium element of the final products should include two valance states of +4 and +5.

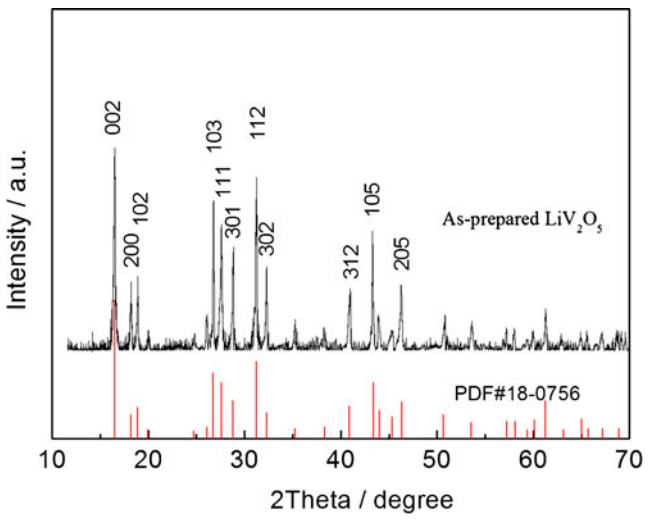

Fig. 2 XRD pattern of as-prepared LiV_2O_5

Figure 4 shows the morphology of as-prepared LiV_2O_5. As observed, the rod-like morphology is almost maintained for LiV_2O_5. However, some individual nanorods of VO_2(B) are partially attached together to form larger and wider ones after high-temperature calcination. Meanwhile, some are broken to form shorter rods. LiV_2O_5 nanorods have an average diameter of 90–250 nm and length of less than 1 μm. Figure 4 depicts the high-resolution TEM image (HRTEM) of individual nanorod, indicating that the nanorod is structurally uniform and free from dislocations and defects. The fringe spacing is 0.636 nm, which is in good accordance with the plane distance of the (100) planes in XRD pattern (Fig. 2). The HRTEM result also demonstrates the single crystalline nature of the nanorods.

FT-IR spectrum gives further insight into the internal structure of as-prepared LiV_2O_5. As can be seen in Fig. 5, the FT-IR result is different from that of V_2O_5 because of the appearance of mixed valence states of vanadium (V^{4+} and V^{5+}) [22]. The sample has characteristic IR peaks at 1,002.9 and 954.4 cm^{-1} which are attributed to V=O stretching of distorted octahedral, while those at 814.9, 783.3, 606.3, and 567.7 cm^{-1} could be due to the vibration of V–O–V bonds.

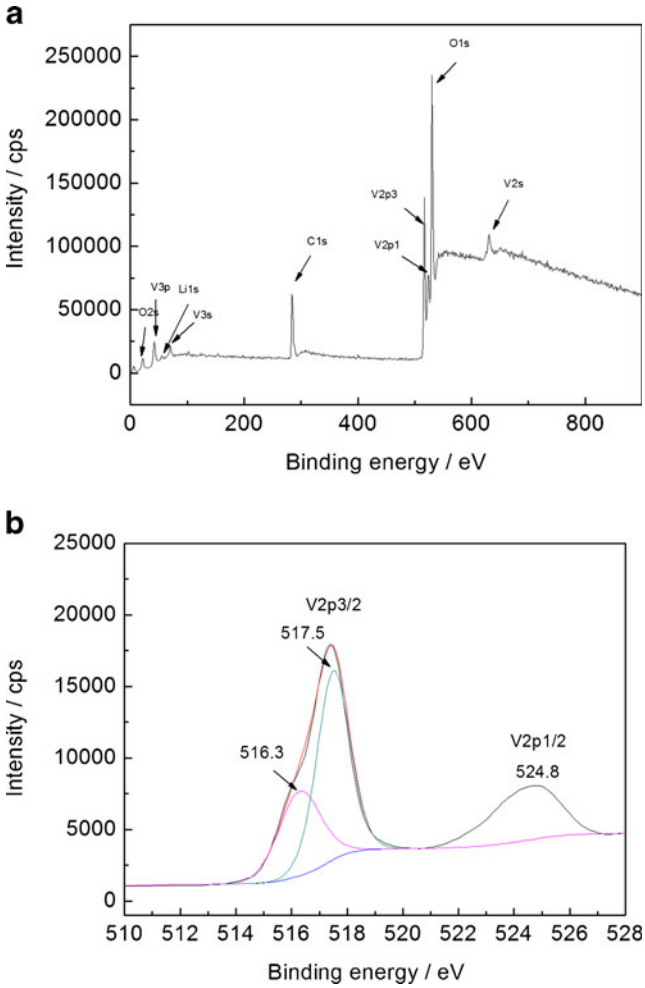

Fig. 3 **a** XPS survey spectrum of as-prepared LiV_2O_5 and **b** the corresponding high-resolution XPS spectrum of V2p region

The FT-IR result is similar to that of LiV_2O_5 as reported by Wang et al. [21, 22].

Cyclic voltammetry curves of LiV_2O_5 nanorods at various scan rates between 2.0 and 4.0 V are shown in Fig. 6. In the anodic curve, three peaks at about 2.53, 3.57, and 3.70 V are observed when the scan rate is 0.2 mV s^{-1}. The corresponding reduction peaks are located at 2.31, 3.42, and 3.53 V, respectively. It should be noted that there are separated reduction peaks between 2.2 and 2.4 V. The splitting of redox peaks was because of the different lithium sites with energy difference for holding the lithium ions [26]. Good lithium ion reversibility is indicated by similar cathodic and anodic peaks. The height and area of the redox peaks are gradually increased with the accelerated scan rate, while the corresponding charges (corresponding to the electrode capacity) remain the same. Figure 7 shows the relationship between the peak current I_p and the sweeping rate of peaks a, b, and c. Good linear dependence suggests that the insertion and extraction process in the LiV_2O_5 is controlled by Li ion diffusion [27]. The Li ion diffusion coefficient could be obtained from Randles–Sevcik equation (Eq. 1) [28]:

$$I_p = \left(2.69 \times 10^5\right) n^{3/2} S C^* D_{Li} v^{1/2} \quad (1)$$

where n is the number of electron transfer in electrode reaction, S is the surface area of electrode (cm^2), D_{Li} is the diffusion coefficient of Li^+ (cm^2 s^{-1}), v is the scan rate (V s^{-1}), C^* is the concentration of Li^+ in $Li_3V_2O_5$ (about 2 Li^+ insertion per formula unit, shown in the following text), 0.028 mol cm^{-3}, which is derived from the crystal volume of 0.3547 nm^3. Based on the fitting linear equations in Fig. 8, the Li ion diffusion coefficients for peaks a, b, and c could be calculated to be 8.71×10^{-9}, 1.49×10^{-10}, and 1.81×10^{-10} cm^2 s^{-1}, respectively. The values are almost of the same magnitude. The Li ion diffusion coefficient of LiV_2O_5 is a little higher than that of LiV_3O_8 [29, 30]. It can be close to that of V_2O_5 [31]. Apparently, LiV_2O_5 nanorods here possess good Li ion diffusion ability, which agrees well with the following electrochemical performance. It is slightly higher than those of the common lithium cathode materials such as $LiMn_2O_4$ and $LiFePO_4$, which have diffusion coefficients of 10^{-9}–10^{-11} cm^2 s^{-1} [32] and 10^{-13}–10^{-14} cm^2 s^{-1} [33], respectively.

Figure 8a shows the relationship of discharge capacity versus the cyclic numbers of LiV_2O_5 nanorods associated with the discharge curves at different cycles. It can be seen that the initial specific discharge capacity is 263.4 mAh g^{-1}. It was increased to 284.3 mAh g^{-1} at the fifth cycle, which corresponds to about 2.0 Li^+ insertion per formula unit, forming $Li_3V_2O_5$. Apparently, the nanorod morphology of LiV_2O_5 benefits the shorter lithium diffusion path and larger contact area between active material and electrolyte, which promises higher discharge capacity. LiV_2O_5 nanorods show stable cycling performance at 15 mA g^{-1}, with a discharge capacity of 270.2 mAh g^{-1} maintained after 15 cycles. The capacity retention is about 97.5% based on the capacity at the second cycle. The electrochemical performance in terms of discharge capacity and cycling stability is much higher than that reported by Wang et al. [22], which is probably ascribed to the different synthesis method and the smaller crystal volume. It is well known that the structure and electrochemical properties of vanadate compounds are greatly associated with their preparation approach. In their report, the initial discharge capacity of γ-LiV_2O_5 was 259 mAh g^{-1} in the potential range of 1.5–4.2 V. However, only 199 mAh g^{-1} remained after 20 cycles. Load curves (Fig. 8b) indicate that the main plateau between 2.6 and 3.8 V contains ca. 125 mAh g^{-1} capacity (44.6% of the total value) in the tenth cycles, which is close to that reported by Barker et al. [23]. The slight splitting of the plateaus at around 3.53 and 2.42 V is well consistent with the

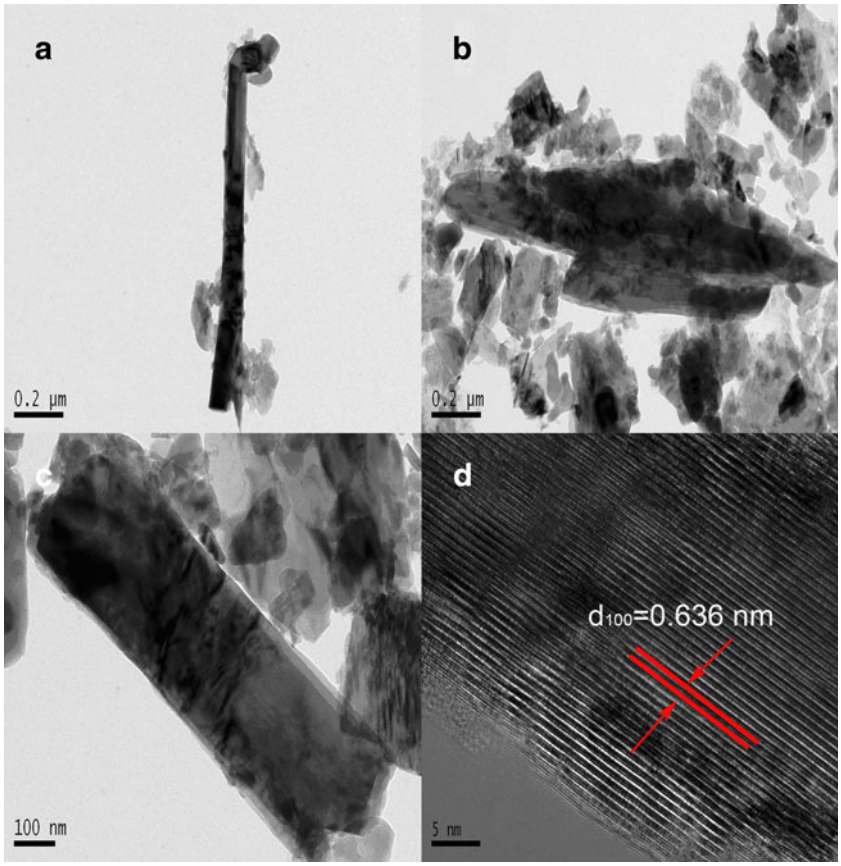

Fig. 4 TEM images (**a**–**c**) and HRTEM image (**d**) of as-prepared LiV_2O_5

CV results. The energy density of electrode material is dependent on the discharge capacity and the corresponding charge–discharge plateau. Therefore, the large capacity at around 3.53 V of γ-LiV_2O_5 would greatly contribute to the higher energy density compared to other vanadates [4, 34]. For example, LiV_3O_8 shows high capacity (more than 300 mAh g^{-1}); however, its main lithium ion insertion/extraction plateaus are concentrated between 2.0 and 3.0 V, which limits its energy density [34].

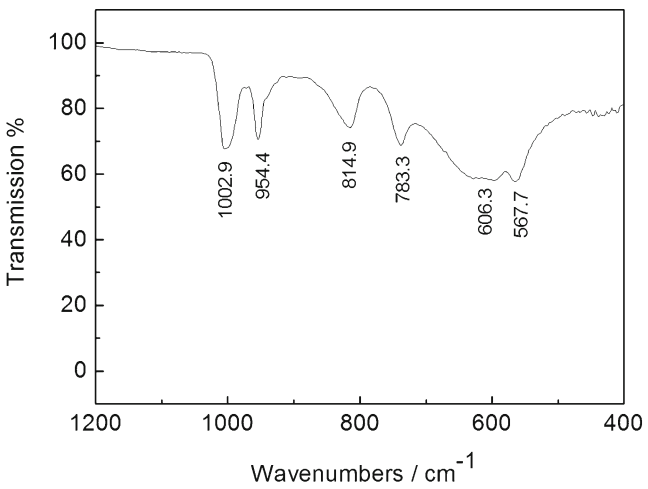

Fig. 5 FT-IR spectrum of as-prepared LiV_2O_5

The cycling performance of LiV_2O_5 nanorod at high current densities (50 and 300 mA g^{-1}) was investigated to measure its rate capability (shown in Fig. 9). The discharge capacity is gradually increased for the first several cycles at 50 and 300 mA g^{-1}, which is probably due to the enhanced electrode polarization at high current densities. Such phenomenon suggests the inferior intrinsic kinetic diffusion ability for LiV_2O_5 in the first several insertion/extraction processes. $NH_4V_3O_8$ also shows the enhanced discharge capacity in our previous work [5, 35]. At 50 and 300 mA g^{-1}, LiV_2O_5 nanorod delivers maximum discharge capacities of 250.1 and 202.6 mAh g^{-1}, respectively. In comparison with that by solvothermal method [22], LiV_2O_5 nanorod exhibits much better rate capability. After 50 cycles, the discharge capacities are decreased to 210.6 and

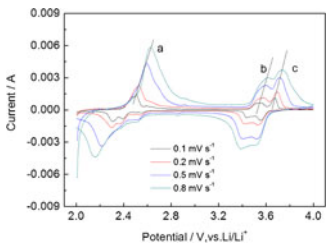

Fig. 6 Cyclic voltammetry curves of as-prepared LiV_2O_5 operated between 2.0 and 4.0 V at various scan rates (0.1, 0.2, 0.5, and 0.8 mV s^{-1})

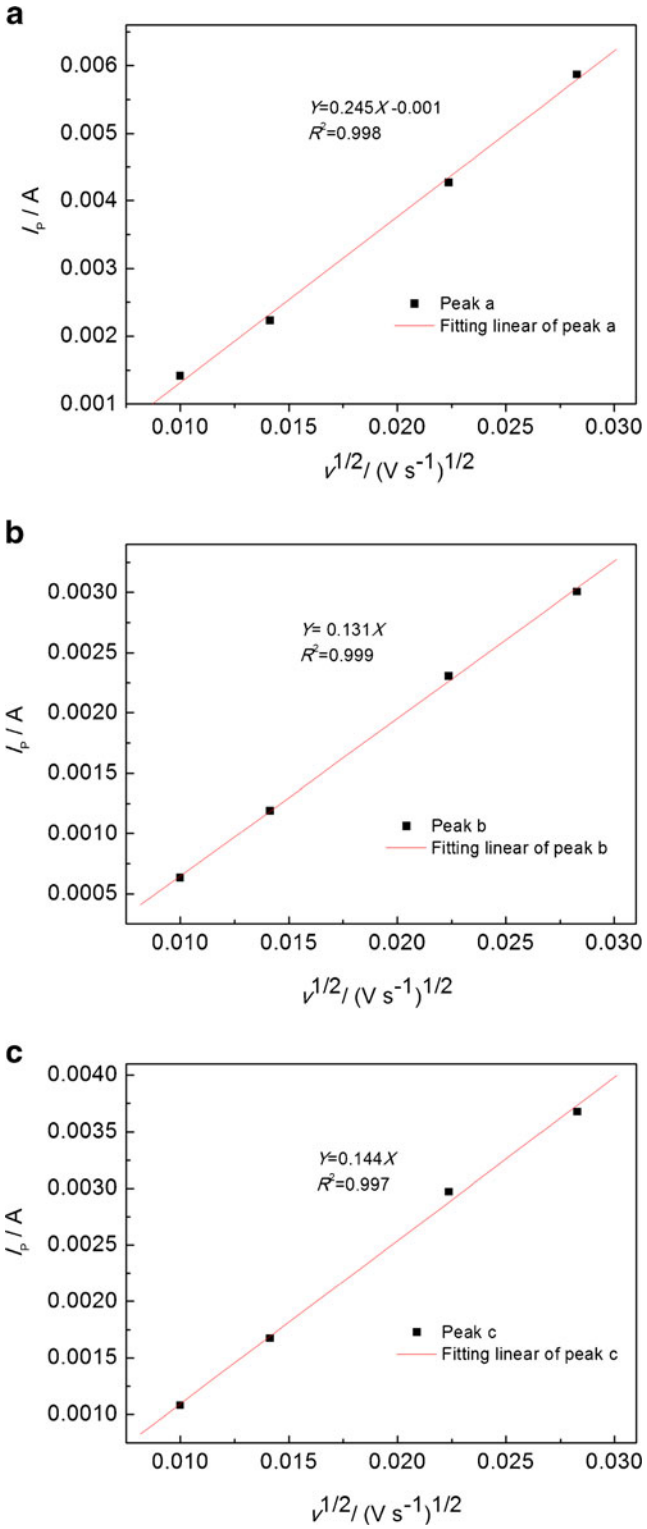

Fig. 7 **a**–**c** Peak current I_p as a function of scan rate $v^{1/2}$ of the cathodic peaks a, b, and c shown in Fig. 6

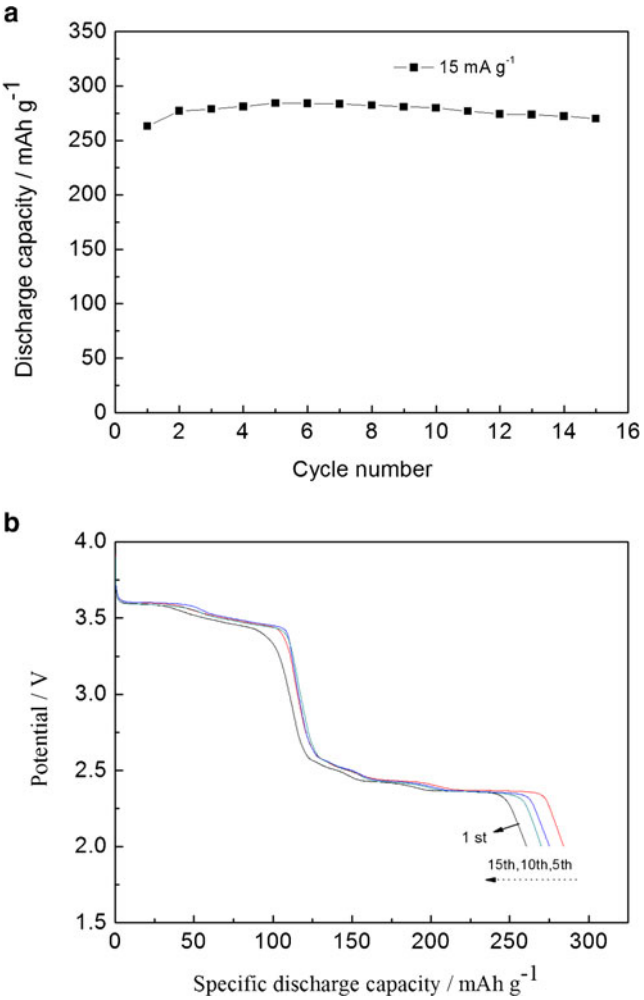

Fig. 8 Cycling performance (**a**) and the corresponding discharge curves (**b**) of LiV_2O_5 nanorods at a current density of 15 mA g^{-1}

162.5 mAh g^{-1}, respectively. The capacity retention at 300 mA g^{-1} is about 84.2% (based on the maximum capacity at the fifth cycle). Generally, vanadates possess relatively poor structure stability due to the variation of phase accompanied by lithium ion insertion and extraction in different voltage ranges. Barker et al. [23] presented the

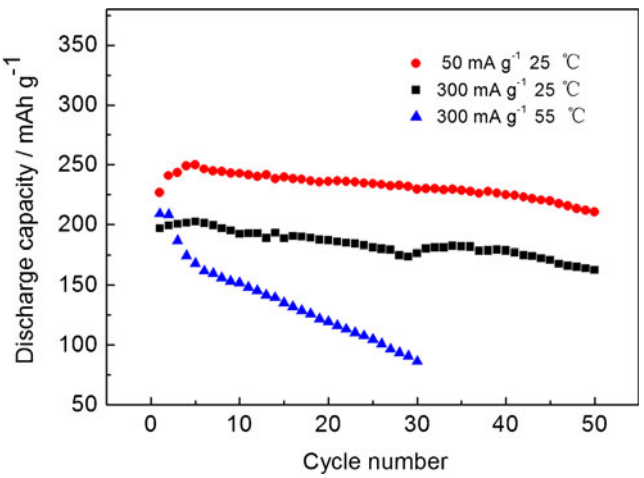

Fig. 9 Cycling performance of LiV_2O_5 nanorods at 50 and 300 mA g^{-1} associated with the high-temperature performance at 55 °C

excellent cycling performance of LiV_2O_5 between 2.8 and 3.8 V. In the present work, the discharge capacity during 2.0–4.0 V (shown in Fig. 8a) also remained well over 15 cycles. However, noticeable capacity loss was found between 2.3 and 2.0 V. It suggests that poor reversibility of lithium ion intercalation and deintercalation in such voltage range is the main reason for capacity loss of LiV_2O_5.

Electrochemical performance of LiV_2O_5 nanorod at elevated temperature was also evaluated in Fig. 9. The initial discharge capacity is 209.1 mAh g^{-1}, a little higher than that at room temperature. However, it is reduced to 86.4 mAh g^{-1} at the 30th cycle with the capacity retention of 58.7% at 55 °C. Obviously, LiV_2O_5 nanorods demonstrate poor cycling stability at high temperature. The trend is consistent with the result reported by Barker et al. [23]. In our previous work, poor cycling stability of $Li_3V_2(PO_4)_3$ at 55 °C was mainly ascribed to the dissolution of vanadium by means of inductively coupled plasma (ICP) [36]. It is well known that vanadate compounds often suffer from poor structural stability when used as lithium intercalation due to vanadium dissolution [37]. Accordingly, we speculate that vanadium ions would gradually dissolve in the electrolyte at elevated temperature, leading to poor cycling performance. Related work is now in progress to improve its high temperature properties.

Conclusions

In summary, γ-LiV_2O_5 nanorods were fabricated by a facile hydrothermal method combined with a solid state reaction. Well-defined VO_2(B) nanorods were used as the precursor. LiV_2O_5 nanorods showed good lithium ion intercalation/deintercalation ability with an Li ion diffusion coefficient of 10^{-10}–10^{-9} cm^2 s^{-1}. It exhibited a high discharge capacity of 284.3 mAh g^{-1} with capacity retention of 97.5% over 15 cycles. At 50 and 300 mA g^{-1}, the discharge capacities of 250.1 and 202.6 mAh g^{-1} were observed, respectively. It also showed good rate capability. A new method was developed to prepare γ-LiV_2O_5 nanorods with high performance for rechargeable lithium batteries.

Acknowledgements The authors greatly appreciate the financial support from the Major State Basic Research Development Program of China (973 Program) (No. 2010CB227204), National Natural Science Foundation of China (No. 50972165), and Research Foundation of Hunan Province for Ph.D. Student (No. CX2010B114), Graduate Degree Thesis Innovation Foundation of Central South University.

References

1. Whittingham MS (2004) Chem Rev 104:4271–4301
2. Spahr ME, Novák P, Scheifele W, Haas O, Nesper R (1998) J Electrochem Soc 145(2):421–427
3. Wadsley AD (1957) Acta Cryst 10:261–267
4. Wang HY, Huang KL, Huang CH, Liu SQ, Ren Y, Huang XB (2011) J Power Sources 196:5645–5650
5. Wang HY, Huang KL, Ren Y, Huang XB, Liu SQ, Wang WJ (2011) J Power Sources 196:9786–9791
6. Chernova NA, Roppolo M, Dillon AC, Whittingham MS (2009) J Mater Chem 19:2526–2552
7. Pinna N, Wild U, Urban J, Schlögl R (2003) Adv Mater 15:329–331
8. Spahr ME, Bitterli P, Nesper R, Müller M, Krumeich F, Nissen HU (1998) Angew Chem Int Ed 37:1263–1265
9. Mao CJ, Pan HC, Wu XC, Zhu JJ, Chen HY (2006) J Phys Chem B 110:14709–14713
10. Cao AM, Hu JS, Liang HP, Wan LJ (2005) Angew Chem Int Ed 44:4391–4395
11. Li BX, Xu Y, Rong GX, Jing M, Xie Y (2006) Nanotechnology 17:2560–2566
12. Li GC, Pang SP, Jiang L, Guo ZY, Zhang ZK (2006) J Phys Chem B 110:9383–9386
13. Chan CK, Peng H, Twesten RD, Jarausch K, Zhang XF, Cui Y (2007) Nano Lett 7:490–495
14. Lee JK, Kim GP, Song IK, Baeck SH (2009) Electrochem Commun 11:1571–1574
15. Zhai T, Liu H, Li H, Fang X, Liao M, Li L, Zhou H, Koide Y, Bando Y, Golberg D (2010) Adv Mater 22:2547–2552
16. Whittingham MS (1976) J Electrochem Soc 123:315–320
17. Delmas C, Cognac-Auradou H, Cocciantelli JM, Menetrier M, Doumerc JP (1994) Solid State Ionics 69:257–264
18. Garcia B, Millet M, Pereira-Ramos JP, Baffier N, Bloch D (1999) J Power Sources 81/82:670–674
19. Baddour-Hadjean R, Marzouk A, Pereira-Ramos JP (2011) J Raman Spectrosc. doi:10.1002/jrs.2984
20. Murphy DW, Christian PA, Disalvo FJ, Waszczak JV (1979) Inorg Chem 18:2800–2803
21. Dai JX, Li SFY, Gao ZQ, Siow KS (1999) Chem Mater 11:3086–3090
22. Wang YW, Xu HY, Wang H, Zhang YC, Song ZQ, Yan H, Wan CR (2004) Solid State Ionics 167:419–424
23. Barker J, Saidi MY, Swoyer JL (2003) J Electrochem Soc 150(9): A1267–A1272
24. Liu HM, Wang YG, Wang KX, Wang YR, Zhou HS (2009) J Power Sources 192:668–673
25. Wagner CD (1979) Handbook of X-ray Photoelectron Spectroscopy. Perkin- Elmer, Minnesota, p 23
26. Kawakita J, Majima M, Miura T, Kishi T (1997) J Power Sources 66:135–139
27. Heli H, Yadegari H, Jabbari A (2011) J Phys Chem C 115:10889–10897
28. Bard AJ, Faulkner LR (2001) Electrochemical Methods, 2nd edn. Wiley, New York, p 226
29. Tossici R, Marassi R, Berrettoni M, Stizza S, Pistoia G (1992) Solid State Ionics 57:227–234
30. Liu EH, Li XH, Hou ZH, He ZQ, Deng LF (2004) Acta Phys Chim Sin 20(4):377–381
31. Mcgraw JM, Bahn CS, Parilla PA, Perkins JD, Readey DW, Ginley DS (1999) Electrochim Acta 45:187–196
32. Cao F, Prakash J (2002) Electrochim Acta 47:1607–1613
33. Prosini PP, Lisi M, Zane D, Pasquali M (2002) Solid State Ionics 148:45–51
34. Xu HY, Wang H, Song ZQ, Wang YW, Yan H, Yoshimura M (2004) Electrochim Acta 49:349–353
35. Wang HY, Huang KL, Liu SQ, Huang CH, Wang WJ, Ren Y (2011) J Power Sources 196:788–792
36. Zhang X, Liu SQ, Huang KL, Zhuang SX, Guo J, Wu T, Cheng P (2011) J Solid State Electrochem. doi:10.1007/s10008-011-1462-0
37. Wang HB, Zeng YQ, Huang KL, Liu SQ, Chen LQ (2007) Electrochim Acta 52:5102–5107